Chemical Physics Letters 575 (2013) 1–11

Contents lists available at SciVerse ScienceDirect

Chemical Physics Letters

journal homepage: www.elsevier.com/locate/cplett

FRONTIERS ARTICLE

Imaging bond breaking and vibrational energy transfer in small water containing clusters

Amit K. Samanta, Lee C. Ch'ng, Hanna Reisler *

Department of Chemistry, University of Southern California, Los Angeles, CA 90089, United States

ARTICLE INFO

Article history:
Available online 14 May 2013

ABSTRACT

This letter presents a brief overview of our recent experimental studies of state-to-state vibrational predissociation (VP) dynamics of small hydrogen bonded (H-bonded) clusters following vibrational excitation. Velocity map imaging (VMI) and resonance-enhanced multiphoton ionization (REMPI) are used to determine accurate bond dissociation energies (D_0) of $(H_2O)_2$, $(H_2O)_3$, $HCl–H_2O$ and $NH_3–H_2O$. Pair-correlated product energy distributions from the VP of these complexes are also presented and compared to theoretical models. Further insights into mechanisms are obtained from the recent quasi-classical trajectory (QCT) calculations of Bowman and coworkers. The D_0 values for $(H_2O)_2$ and $(H_2O)_3$ are in very good agreement with recent calculated values, and the results are used to estimate the contributions of cooperative interactions to the H-bonding network.

1. Introduction

Scientists have been fascinated with the nature and dynamics of hydrogen bonded (H-bonded) networks from the early 1920s [1–7]. In the gas phase, emphasis has been placed on investigations of clusters in the cold environment of molecular beams, with most reports focused on spectroscopy [8–16]. The bond breaking mechanisms via vibrational predissociation (VP) of H-bonded complexes of water, which are the focus of the present article, are at present much less well understood [10]. Alan Pine and Roger Miller were among the first to extend the spectroscopic work on dimers to state-specific VP, using $(HF)_2$ and $HF–C_2H_2$ as benchmark cases [10,17–23].

The prototype for H-bonded clusters is the water dimer, whose atmospheric importance continues to be the subject of much interest [24–27]. In this context, an accurate value of the bond dissociation energy (D_0) of the dimer is crucial in assessing the contributions of the water dimer to absorption and detection in the atmosphere [24,25,28,29]. In addition, the pairwise interactions of water monomers in the dimer are important in elucidating the behavior of water in larger networks for which non-pairwise (cooperative) interactions have significant contributions. Thus, describing correctly the structure and dynamics of small clusters of water has been a long-standing goal of both theory and experiment.

It was quite surprising to us when we initiated our work to realize that very little was known about the VP dynamics of simple H-bonded dimers and trimers of polyatomic molecules [10,18–20,22]. In fact, even the bond dissociation energies of dimers that have become benchmarks for theory [e.g. $(H_2O)_2$, $(NH_3)_2$, $HCl–H_2O$] have not been known with sufficient accuracy. At the same time, because of the relevance of H-bonded networks to environments ranging from biological molecules in cells to gaseous species erupting from icy bodies in the solar system, theoretical efforts have been intense, and today it is possible to generate accurate potential energy surfaces (PESs) for small clusters, such as those of water and ammonia, in order to better describe the behavior of liquids and ices [30–49]. For example, the surface of amorphous solid water has large contributions from pairwise interactions [50], and solid ammonia-water interfaces are implicated in the surface chemistry of icy planets [51].

While spectroscopic measurements give benchmark data on rotational constants and vibrational frequencies that can test PESs near equilibrium, there is only scant experimental information on bond dissociation energies and energy flow dynamics in vibrationally excited clusters that probes the far reaches of the PES or its repulsive regions. So far, quantum dynamical calculations on accurate PESs that describe VP have been carried out only for the simplest dimers with an atom or a diatom as a subunit [9,11,31,35,37].

It is impossible in a single review or, for that matter, in a single book, to capture all the intriguing aspects of the behavior of water. Water clusters alone merit a monograph. This letter is focused on one aspect: recent experimental studies of VP dynamics of small H-bonded clusters that include water. In the past few years we have exploited the photofragment imaging technique to study the VP of small H-bonded dimers in molecular beams [52–61]. Specifically, we used vibrational excitation of intramolecular modes and velocity map imaging (VMI) to determine D_0 and study VP in dimers in which at least one of the monomers is a polyatomic

* Corresponding author. Fax: +1 213 740 3972.
E-mail address: reisler@usc.edu (H. Reisler).

0009-2614/$ - see front matter © 2013 Elsevier B.V. All rights reserved.
http://dx.doi.org/10.1016/j.cplett.2013.05.003

molecule. The imaging methodology provides accurate D_0 values ($\pm 10\ cm^{-1}$) as well as fragment rovibrational energy distributions. The latter give information on energy transfer pathways within the dimer subunits and across the H-bond, as well as couplings to intermolecular vibrational modes. Moreover, by recording images of selected rovibrational levels of one fragment, the experiments provide *pair-correlated energy distributions*, i.e., the rovibrational energy distribution of one fragment correlated with a selected quantum state of the other, which provides more stringent tests of mechanisms [61].

Because of the disparity between the frequencies of inter- and intramolecular vibrational modes, vibrational energy transfer in small clusters is usually inefficient, giving rise to nonstatistical VP dynamics and state-specificity in fragments' rovibrational populations [10]. As a starting point in interpretations, we use the qualitative propensity rules proposed by Ewing for describing predissociation rates [62,63]. These are based on momentum (or energy) gap laws and predict a preference for fragment channels in which the number of transferred quanta in the dissociation is minimized. In general, there is a preference for vibrational excitation over rotational excitation over translational energy release. Since a small change in the number of vibrational quanta can absorb the greatest amount of energy, disposal of energy by vibrational excitation is the most favorable. Referring to rotational excitation and translational energy release, the effective quantum number change in translational energy release is greater than in rotational excitation, provided the moments of inertia of the fragments are not too large. Therefore, rotational excitation is usually more favorable than translational energy release in our dimers studies, for which the fragments' moments of inertia are small. The Ewing model describes correctly the VP rate in a large number of dimers, and explains why VP often results in high vibrational excitation in fragments and small translational energy (E_t) release. The question of vibrational state specificity is not addressed in this model, nor does angular momentum conservation restrict product rotational excitation.

The complementary angular momentum model proposed by McCaffery and coworkers is centered on linear-to-angular momentum interconversion [57,64,65]. It has been used successfully to describe rotational state distributions in inelastic collisions and, more recently, in the VP of weakly bound dimers [54,57]. Realizing that there is insufficient anisotropy in the long-range part of the PES of weakly bound complexes to explain the observed high fragment rotational excitation, the involvement of the repulsive, hard-shaped part of the PES is invoked. The model identifies the principal geometries and impact parameters from which dissociation occurs by fitting to experimental results.

However, exit-channel energy transfer may modify the initial distributions, especially when energy differences between rotational levels are small. This can lead to Boltzmann-like rotational distributions, though they usually deviate from statistical predictions by exhibiting enhanced populations of high rotational levels. These propensities are most clearly revealed in pair-correlated rotational distributions [10,57].

For statistical-like systems, the most useful model is phase space theory (PST). PST applies conservation of energy and angular momentum and, most importantly, assumes that all allowed states are equally populated [66–68]. Throughout this letter, we present examples of the applicability for these models to different clusters. We also make comparisons with the results of recent quasi-classical trajectory (QCT) calculations.

Referring to fragment vibrational excitation in VP of polyatomic dimers, we find that the existing propensity rules cannot explain the exquisite state specificity observed even among those vibrations that are associated with small E_t release. It appears that despite the flexibility of the monomers, energy transfer is restricted. Full dynamical calculations on accurate PESs are therefore essential to explain the observed product state distributions. This is still a challenging task in spite of the availability of accurate PESs for simple dimers such as the water dimer. The reasons are the anharmonicity of the intermolecular vibrations, the small coupling matrix elements between the excited intramolecular stretch vibration to the intermolecular vibrations that lead to VP, the long lifetimes of the dimers (up to several nanoseconds), and the need to include both the long range and the repulsive parts of the PES. Clearly, synergistic efforts by theory and experiment are needed to refine our understanding of the VP of H-bonded dimers and larger clusters, and below we describe the very recent efforts by Bowman and coworkers on the VP of the water dimer and trimer.

There are several issues to resolve regarding energy disposal in VP: (i) How does vibrational energy flow from the excited H-bonded stretch of the donor to the reaction coordinate? (ii) What determines rotational and vibrational excitation in the fragments? and (iii) How is energy shared between the donor and the acceptor?

In discussing bond dissociation energies, a distinction is made between the binding energy, D_e, which is the ground state minimum, and D_0, which includes zero point energy (ZPE). The former is obtained in electronic structure calculations but cannot be measured experimentally. The latter can be determined experimentally but calculating ZPE of clusters poses theoretical challenges because of the need to include anharmonicity of intermolecular modes and the flexibility of the monomers.

The article is organized as follows. In Section 2 we describe the experimental method and illustrate it with the determination of D_0 for the HCl–H_2O dimer. In Section 3 we summarize our joint experimental and theoretical studies of the VP of the water dimer and trimer, and in Section 4 we examine the VP of the heterodimers HCl–H_2O and NH_3–H_2O. Finally, in Section 5 we present conclusions and perspective.

2. Experimental approach

The experimental approach is best illustrated with the VP of HCl–H_2O in which water fragments are probed state selectively [58]. For our experiments to be successful, several requirements must be met: (i) The desired cluster IR spectrum must be separated from the monomer and from other clusters; (ii) A reliable resonance enhanced multiphoton ionization (REMPI) detection scheme must exist for at least one of the monomer fragments and display isolated rovibrational levels suitable for imaging; (iii) The images should have distinct structures and/or clear energy cutoffs that can be used to determine D_0 accurately; (iv) The clusters must be generated at sufficient concentrations in the expansion. Of these requirements, (ii) turned out to be the most challenging.

The experimental arrangement is shown schematically in Figure 1. A molecular beam containing HCl and H_2O seeded in He carrier gas is expanded into the vacuum chamber. The HCl stretch vibration of the dimer is excited by an IR laser tuned to the peak of the absorption band of the dimer ($\sim 2723\ cm^{-1}$). Since the vibrational energy exceeds the dimer's D_0, the dimer dissociates producing HCl and H_2O fragments in a distribution of rotational states (in this case the available energy is insufficient to excite the vibration of either fragment.). A tunable UV laser ionizes H_2O fragments in selected rotational J''_{KaKc} levels, and the selected fragments are detected by a position-sensitive detector, creating a 2-dimensional projection of the 3-dimensional velocity (speed) distribution. The recorded images are reconstructed to generate the 3-dimentional velocity distributions from which the center-of-mass (c.m.) translational energy release is determined [69].

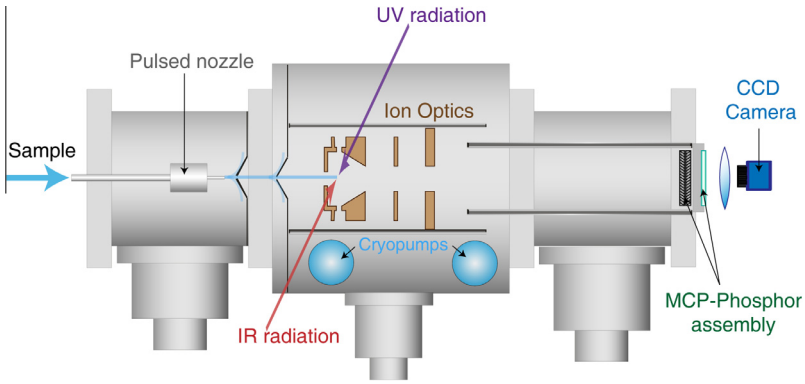

Figure 1. Schematics of the experimental arrangement.

Three separate experiments are carried out: (1) By selecting a specific J''_{KaKc} of H_2O and scanning the wavelength of the IR laser, an action spectrum of the dimer is obtained (i.e. a partial absorption spectrum correlated with the monitored product level, as shown in Figure 2); (2) By fixing the IR laser wavelength to coincide with the peak of the absorption spectrum and scanning the UV laser in the region of 2-photon absorption to the $\tilde{C}^1B_1$ state of H_2O (or D_2O), a 2 + 1 REMPI via the $\tilde{C}^1B_1\,(000) \leftarrow \tilde{X}^1A_1\,(000)$ transition is obtained from which rotational states of the H_2O fragment are identified (Figure 3); (3) By selecting both J''_{KaKc} of H_2O and the peak infrared absorption of the dimer, an image is recorded from which the velocity (speed) or E_t distribution of the fragments is derived (Figure 4).

Experiment (1) confirms that the detected fragments are correlated only with dimer absorption, without contributions from larger clusters. Experiment (2) serves to locate isolated rovibrational levels of the monomer fragment that are suitable for imaging. For experiment (3) we use VMI to obtain the speed distribution of the detected fragment. The VMI arrangement consists of a four-electrode ion acceleration assembly, a 60-cm field-free drift tube, and a microchannel plate (MCP) detector coupled to a phosphor screen that is monitored by a CCD camera (Figure 1) [70,71]. Speed distributions are obtained by summing over the angular distribution for each radius in the reconstructed image, and are converted to c.m. E_t distributions using momentum conservation, the appropriate Jacobian, $(\propto E_t^{-1/2})$, and calibration constants obtained from other experiments. The c.m. E_t distributions are analyzed to determine the internal energy distributions of the HCl co-fragments as well as D_0 of HCl–H_2O. The large spike in the image with near zero kinetic energy is due to the monomer in the molecular beam, and is ignored in the fittings.

Rotational state populations of pair-correlated HCl fragments are best derived from velocity (speed) distributions (Figure 4); this approach makes it easier to resolve structures at low E_t and identify the maximum observed E_t. Fitting is accomplished by assigning a GAUSSIAN-shaped curve to each rotational state of HCl with a width characteristic of the experimental resolution. The positions of the GAUSSIANS are determined by varying D_0 until the best fit is obtained. The separation between adjacent GAUSSIANS is determined from the known rotational constants of HCl. The heights of the GAUSSIANS are first described by an exponentially decaying smooth function of E_t, e^{-DEt} where D is a fitting parameter and E_t is the c.m. translational energy. Whenever possible, after fitting using a smooth exponential function, the GAUSSIANS heights are individually adjusted to obtain the final best fits.

Since in this case the vibrational modes of neither monomer fragment are energetically accessible, $E_{vib}(HCl)$ and $E_{vib}(H_2O)$ are set to zero in the energy conservation equation, resulting in:

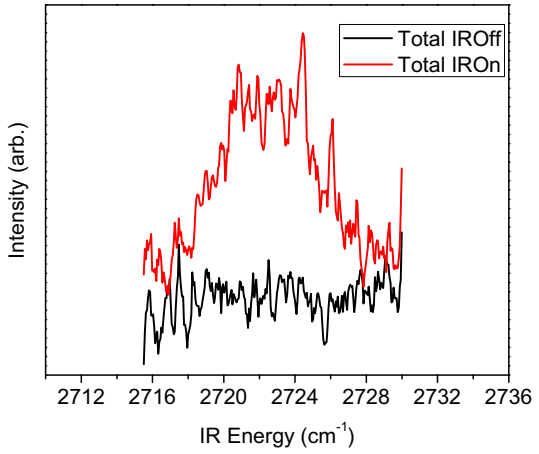

Figure 2. Fragment yield IR spectrum of the HCl–H_2O dimer obtained by monitoring the $H_2O(000)$ photofragment. The black line shows the background signal from H_2O monomer in the molecular beam under the same conditions.

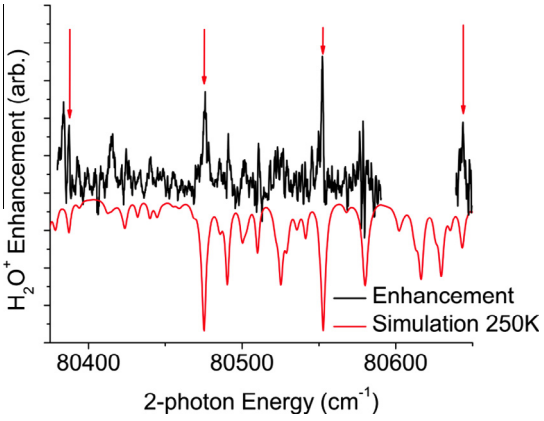

Figure 3. H_2O photofragment 2 + 1 REMPI enhancement spectrum obtained by exciting the HCl stretch of HCl–H_2O at 2723 cm^{-1} and scanning the UV laser through the region of the $\tilde{C}^1B_1\,(000) \leftarrow \tilde{X}^1A_1\,(000)$ transition of H_2O. The simulated spectrum at $T = 250$ K obtained using PGOPHER [76] is shown in red. The gap in the data corresponds to the region of low J transitions for which the background intensity is too large to measure enhancement. [Adapted with permission from Ref. [58] (Copyright 2011 American Chemical Society)].

$$E_{int}(HCl - H_2O) + h\nu = D_0 + E_t + E_{rot}(HCl) + E_{rot}(H_2O; J''_{K_aK_c})$$

where E_{int}(HCl–H_2O) is the internal energy of the dimer prior to excitation, hν is the photon energy used for vibrational excitation

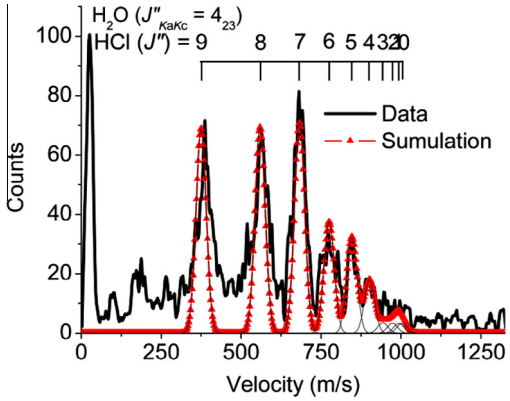

Figure 4. Velocity distribution obtained by monitoring $H_2O(000)$ $J''_{KaKc} = 4_{2,3}$. The red line corresponds to the total fit, where each peak corresponds to a specific HCl(J) level of the HCl cofragment, calculated by using energy conservation and the known rotational constants of HCl. [Adapted with permission from Ref. [58] (Copyright 2011 American Chemical Society)].

of the dimer (2723 cm^{-1}), E_t is the (measured) c.m. translational energy, $E_{rot}(H_2O; J''_{KaKc})$ is the rotational energy of the monitored H_2O fragment, and E_{rot}(HCl) is the rotational energy of HCl, which is related to E_t by energy conservation. The internal energy of the dimer, E_{int}(HCl–H_2O), is estimated to be 1 ± 1 cm^{-1} from $T = 5$ K in the molecular beam. State selection in the REMPI detection defines $E_{rot}(H_2O; J''_{KaKc})$ and E_t is determined from the images. This procedure, when followed for several J''_{KaKc} levels of the water fragments, establishes D_0 accurately, $D_0 = 1334 \pm 10$ cm^{-1}.

3. Vibrational predissociation of the water dimer and trimer

There is no need to expand on the importance of H-bonding in water in our solar system, but water is important not only as a bulk solvent and ice; it is also a player in constrained environments such as clusters, nanoparticles, molecular wires and bridges, inside nanotubes and proteins, to name but a few. The pioneering work of Saykally and coworkers [26,27,72–75] on the vibrational–rotational–tunneling (VRT) levels of ground state water dimers [$(H_2O)_2$ and $(D_2O)_2$] and larger clusters has been seminal to our understanding of ground state motions in small water clusters, and has served as benchmarks for testing and refining PESs of clusters and condensed phases. Absent from the joint theoretical–experimental effort until very recently was an accurate experimental determination of D_0 of the water dimer and trimer. These values were available from recent high level calculations but they needed experimental verification.

3.1. The water dimer: breaking the hydrogen bond

Our imaging experiments were the first to determine D_0 of the water dimer with spectroscopic accuracy [59]. With Bowman and coworkers we also published the first detailed theoretical and experimental investigation of the H-bond breaking dynamics in H_2O and D_2O dimers [60]. Upon vibrational excitation of the H-bonded OH(D) stretch fundamental of the dimers, two channels are energetically open for $(H_2O)_2$ and $(D_2O)_2$: (000) + (000) and (000) + (010), where (000) and (010) are the ground and first bending level of the water fragment, respectively.

The main experimental difficulty in these studies is that no good REMPI scheme exists for state-specific detection of water fragments. In our work we used 2 + 1 REMPI spectroscopy of H_2O and D_2O fragments via the $\tilde{C}^1B_1$ (000) ← $\tilde{X}^1A_1$ (000 and 010) transitions, but this optical detection system is far from ideal. The $\tilde{C}^1B_1$ excited state of H_2O is more predissociative than that of D_2O but the D_2O spectrum is more congested [76]. Thus, each system presents different experimental challenges. Background from ambient water is another problem, especially when monitoring water in the ground vibrational state, but the problem is much diminished when probing fragments in the (010) level. In spite of the fast predissociation in the H_2O $\tilde{C}^1B_1$ state, several isolated transitions of (000) and (010) fragments suitable for imaging do exist, and images obtained from selected rotational levels of H_2O (000), H_2O (010), and D_2O (010) fragments were used for an accurate determination of D_0. Representative velocity distributions obtained for selected rovibrational transitions of H_2O and D_2O are shown in Figure 5.

Although a large number of water cofragment rotational levels are energetically correlated with each probed water level, distinct structures are present in all the images, as evident in Figure 5. The structures in all the images must be fit with a single D_0 value. This constrains the fits to a unique value, and we obtain $D_0 = 1105 \pm 10$ and 1244 ± 10 cm^{-1} for H_2O and D_2O, respectively. The fits have error bars of only a few cm^{-1} but additional uncertainties in the internal energy of the dimer and excitation wavelength calibration increase the error bars to ± 10 cm^{-1}.

High-level electronic structure models are capable today of calculating D_e accurately, and there is quite good agreement among D_e values obtained by different groups [26,43,77–82]. These values are clustered around a value of $D_e = 1700$ cm^{-1} with a range of about ± 100 cm^{-1}. To obtain D_0 the difference between the ZPEs of the dimer and the monomer fragments needs to be evaluated. The recent high level calculations of Bowman and coworkers give $D_0 = 1103$ and 1244 cm^{-1} for $(H_2O)_2$ and $(D_2O)_2$, respectively, in excellent agreement with the experimental results [81,83]. They were carried out at the CCSDT(T)/aug-ccpVTZ level of theory/basis set with the addition of several modifications to the PES. The ZPE is determined by a Diffusion Monte Carlo (DMC) calculation, which appears to capture the anharmonicity in the potential and the large amplitude zero point motions in the flexible monomers. Very recently, Leforestier et al. used a new 12-dimensional PES with flexible monomers (called CCpol-8sf) and reported $D_0 = 1108.2$ cm^{-1} [84], again in excellent agreement with our experimental value. A corresponding value obtained with the rigid PES CCpol-8s, $D_0 = 1094$ cm^{-1}, has a greater deviation, demonstrating that a flexible monomer PES improves the agreement.

A much more challenging task is elucidating energy transfer pathways leading to H-bond breaking and the detailed mechanism of VP. As noted above, fully quantal calculations are still beyond reach for polyatomic dimers with many coupled exit channels. The good fits for fragment rotational distributions obtained by using a classical model with hard-shaped potentials show that the repulsive part of the PES is involved but the model is not usually predictive [57]. An important step toward the goal of describing the VP dynamics are the QCT calculations of Czakó and Bowman, carried out recently on their high level HBB2 PESs for $(H_2O)_2$ and $(D_2O)_2$ [83].

In the QCT calculations, standard normal mode sampling was applied to prepare the initial states by giving harmonic ZPE to each mode and an extra quantum of excitation to the bound OH(D) stretch fundamental, i.e., almost a local mode of the donor. The correlated rovibrational distributions were computed by the GAUSSIAN binning procedure (1 GB). 1 GB means one GAUSSIAN weight for each fragment based on its total vibrational energy. It also assigns small weights for trajectories in which either fragment violates ZPE, thereby effectively addressing the ZPE issue of the QCT method.

The experimental and theoretical results on product state distributions are complementary. Imaging experiments provide pair-correlated product state distributions, whereas QCT calculations give the total rotational distributions in each fragment. Both

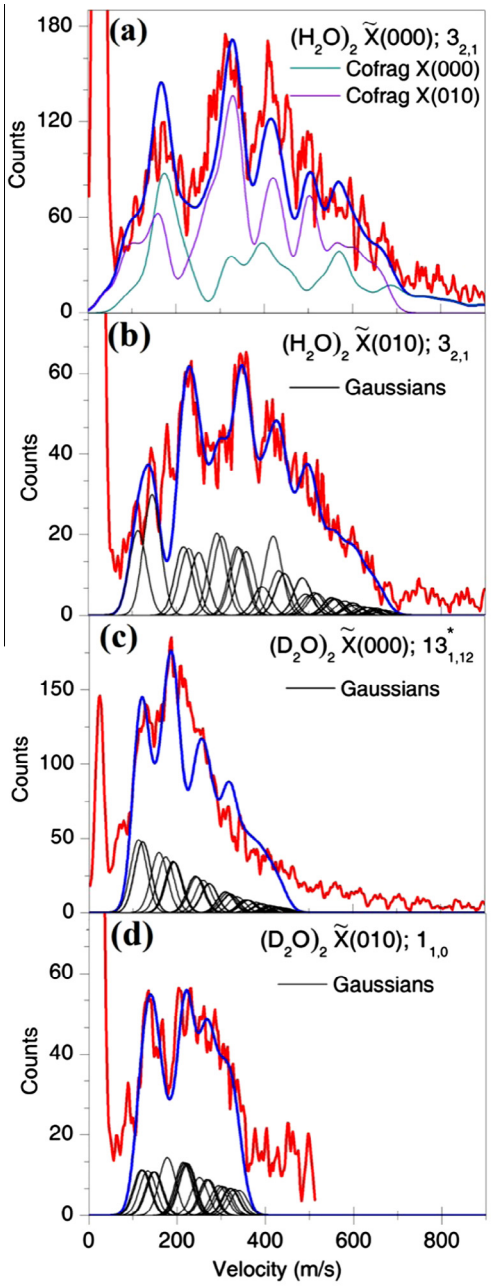

Figure 5. Velocity distributions obtained for selected rovibrational transitions of H_2O and D_2O (red curves) from VP of $(H_2O)_2$ and $(D_2O)_2$. The gaussians (black curves) in (b), (c) and (d) are the energetically allowed rotational levels of the cofragment and the blue lines are the summation of those gaussian curves. In (a) the gaussians (not shown) were integrated to obtain the green and purple curves for cofragments in the (000) and (010) state, respectively. In (c) *indicates a blended transition with major contribution from $J''_{KaKc} = 13_{1,12}$. In (b) and (d), after fitting with a smooth exponential function, we further adjusted the gaussian heights individually to obtain the final best fits. [Adapted with permission from Ref. [60] (Copyright 2012 American Chemical Society)].

experiment and theory show that dissociation generates products in rotational states encompassing all the energetically allowed levels. The overall calculated rotational distributions peak at fairly low rotational levels. Figure 6 shows a comparison of the pair correlated velocity distribution obtained by monitoring H_2O (010) $J''_{KaKc} = 3_{2,1}$ and the simulation generated by PST calculation. Their clear disagreement indicates a non-statistical behavior of the experimental rotational distribution. There is a preference for populating high rotational levels that minimize E_t release, in agreement with the Ewing model. What the experiments cannot establish, but which is revealed in calculations, is that the rotational distributions in the original donor and acceptor fragments are similar for both the (000) + (010) and (000) + (000) dissociation channels of $(H_2O)_2$ and $(D_2O)_2$.

In addition, the QCT calculations predict, in agreement with experiment, that the predominant VP channel in $(H_2O)_2$ and $(D_2O)_2$ is (000) + (010), though the experiments reveal a somewhat larger contribution from the (000) + (000) channel. For $(D_2O)_2$ large contributions from high rotational levels in the (000) fragments are observed that have similar energies to the (010) bending level.

The experimental and theoretical results suggest the following scenario for the VP dynamics of the water dimer. Following excitation of the H-bonded OH(D) stretch of the donor, vibrational energy is shared between the donor and acceptor vibrational levels before dissociation takes place. The major dissociation channel is (000) + (010) with equal probability of the bending excitation to reside in the donor and acceptor fragments. The donor and acceptor have similar and broad rotational state distributions. The pair-correlated distributions are also broad, with a nonstatistical rotational energy distribution in the cofragment biased in favor of high rotational levels that minimize E_t release.

The initial pathways of energy transfer out of the excited OH(D) stretch are not yet elucidated. In the first step, the excited bonded OH stretch vibration possibly couples to two quanta of intramolecular bend and one or more intermolecular vibrations, since there are near-resonant pathways for such coupling for both $(D_2O)_2$ and $(H_2O)_2$. This energy must then transfer to the intermolecular modes, including the dissociation coordinate, a process which most often leaves one quantum of bending excitation in a fragment. One can envision scenarios where the initial bending excitation resides in one water molecule or is shared between the two water molecules (i.e. formation of (020) or (010) + (010)).

More insight is obtained by examining the time evolution of trajectories that lead to dissociation, and $(H_2O)_2$ and $(D_2O)_2$ trajectories can be seen as animations in Ref. [60]. In addition, snapshots of a representative $(H_2O)_2$ trajectory are shown in Figure 7. The trajectories show that the identity of the donor and acceptor switches several times before dissociation occurs several picoseconds later.

The required couplings of at least one bending quantum to the intermolecular modes are likely to give rise to some intramolecular vibrational redistribution among the intermolecular modes, including the exchange of donor and acceptor, which can explain their final broad and similar rotational state distributions. As is common to most small dimers, the coupling to the dissociation coordinate is inefficient, with dimer lifetimes > 10 ps. However,

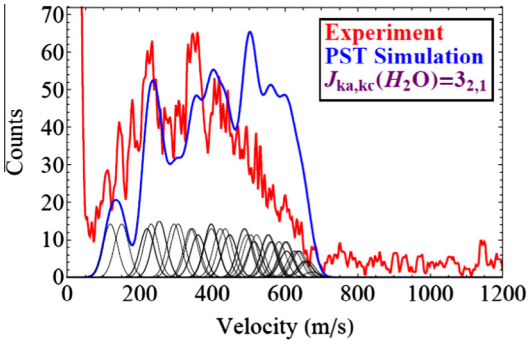

Figure 6. Velocity distribution from reconstructed image obtained by monitoring H_2O $X(010)$ $J''_{KaKc} = 3_{2,1}$ fragments from $(H_2O)_2$ (red curve). The blue curve corresponds to a statistical velocity distribution, calculated by using PST, which does not fit the experimental distributions.

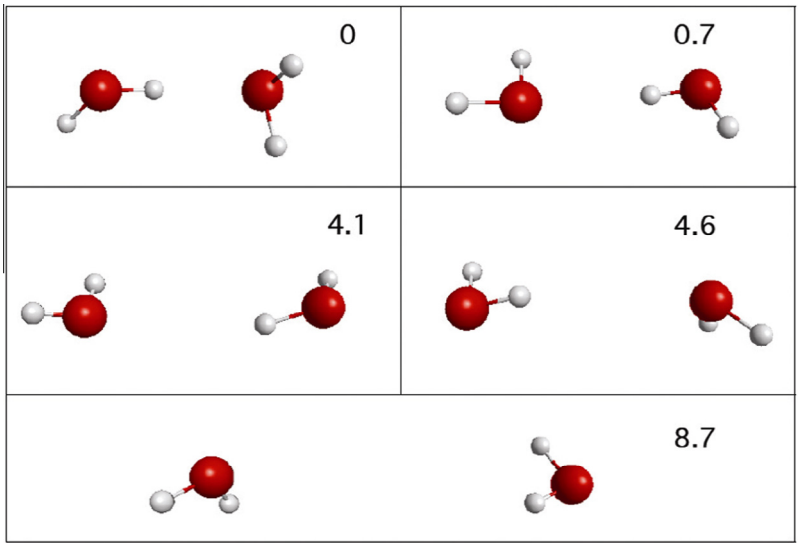

Figure 7. Snapshots of water dimer trajectories leading to dissociation of $(H_2O)_2$. The frames are labeled in picoseconds from initiation. [Adapted with permission from Ref. [60] (Copyright 2012 American Chemical Society)].

even though there is ample time for the energy to redistribute among the available vibrational states, only restricted paths lead eventually to dissociation. Inspection of several trajectories leading to VP shows that exchanges of donor and acceptor occur several times during the trajectory, which explains the similar rotational distributions as noted above. The minor (000) + (000) channel may result in part from processes in which the excited dimer samples the repulsive part of the PES in an impulsive interaction, converting both bending quanta into fragment rotation and translation, thereby accessing the high rotational levels observed in the VP of $(D_2O)_2$.

3.2. The water trimer: contributions from cooperative interactions

The water trimer constitutes the smallest network of water molecules, but in spite of the fundamental interest in the nature of the cooperative interactions in H-bonded networks and their influence on the H-bond strength, no experimental measurements of D_0 of the trimer have been reported. Likewise, H-bond breaking pathways have not been elucidated. Below, we present results of our first joint experimental and theoretical study, carried out in collaboration with Wang and Bowman [85].

The structures, vibrational frequencies, PES, three-body effects, binding energies and tunneling motions of the water trimer have been studied extensively by theory and experiment. Work up to 2003 is summarized in a comprehensive review [74], and additional work can be found in Refs. [86–92]. The high-resolution spectroscopic studies of Saykally and coworkers mapped in detail VRT levels of the trimer and estimated the barriers between different conformations. In addition, the intra- and intermolecular vibrational modes were characterized in molecular beams, He droplets and matrix isolation experiments [73,93–98].

Upon excitation of the H-bonded OH stretch vibration (3536 cm^{-1}), the energy imparted to the trimer is sufficient only for dissociation to $H_2O + (H_2O)_2$ [99]. We have examined the pair-correlated fragment state distributions by monitoring the H_2O monomer fragment, which can be formed only in the ground (000) vibrational state. In contrast, all the intermolecular vibrational modes of the $(H_2O)_2$ fragment can be populated (but not the intramolecular modes). The experimental excitation and detection scheme is shown in Figure 8.

The water trimer adopts six low-lying stationary points [99]. Among these, the global minimum (Figure 9) consists of three H-bonds, and the cyclic structure is conventionally denoted as 'up–up–down' depending on the orientations of the free OH-bonds relative to the plane defined by the three oxygen atoms. $(H_2O)_3$ has one weaker H-bond due to repulsion of the two 'up' OH-bonds, giving two different H-bonded OH-stretch fundamentals that differ in energy by 12–15 cm^{-1}, but these are not distinguished in our experiments. The fundamental transition of the H-bonded OH-stretch of $(H_2O)_3$ has been previously characterized, and in their gas phase molecular beam experiments, Huisken et al. assigned the transitions of $(H_2O)_2$, $(H_2O)_3$, and $(H_2O)_4$ at 3601, 3533, and 3416 cm^{-1}, respectively.

The REMPI spectrum of H_2O fragments in the $\tilde{C}^1B_1$ (000) ← $\tilde{X}^1A_1$ (000) band produced by VP of $(H_2O)_3$ at 3536 cm^{-1} was simulated fairly well with a rotational temperature of 230 ± 70 K,

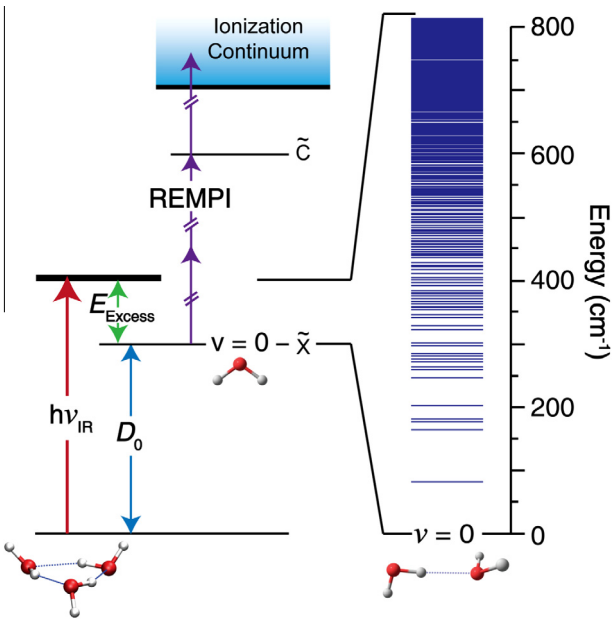

Figure 8. Experimental scheme for vibrational predissociation of the water trimer.

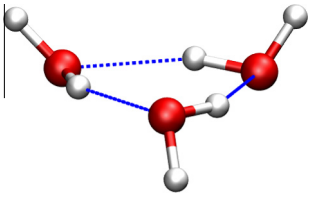

Figure 9. Minimum energy structure of the water trimer denoted as 'up–up–down'.

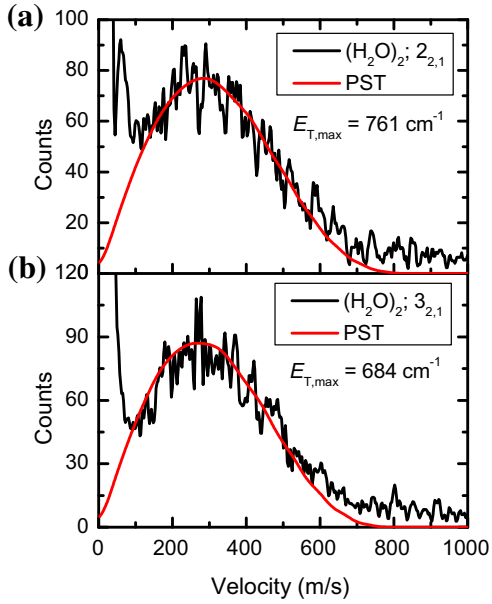

Figure 10. Velocity distributions from reconstructed images obtained by monitoring $H_2O(000)$ fragments in J''_{KaKc} = (a) $2_{2,1}$ and (b) $3_{2,1}$ from VP of $(H_2O)_3$. Black curves show experimental measurements and red curves correspond to best fits obtained by using statistical distributions calculated by PST with D_0 as an adjustable parameter (see the text for details). [Adapted with permission from Ref. [85] (Copyright 2013 American Chemical Society)].

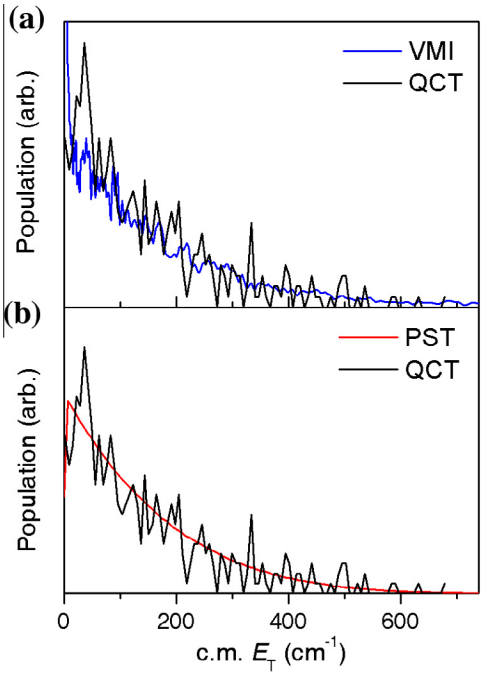

Figure 11. Comparison of the translational energy distribution calculated by QCT, where the H_2O fragments are in J''_{KaKc} = 2–4, with (a) the distribution determined by VMI by detecting H_2O fragments in $J''_{KaKc} = 3_{2,1}$, and (b) statistical distribution obtained by PST. [Adapted with permission from Ref. [85] (Copyright 2013 American Chemical Society)].

corresponding to 160 ± 50 cm^{-1}. Figure 10 shows two speed distributions obtained by VMI by monitoring isolated rotational levels of the H_2O fragments. In contrast to the speed distributions measured in the VP of H_2O and D_2O dimers (as well as water dimers with other small molecules), which show distinct structures in the speed distributions, there are no reproducible structural features in Figure 10. Therefore, our estimated D_0 value for the cyclic trimer is less precise (see below).

We expected the product energy distributions in VP of $(H_2O)_3$ to be more statistical than in small dimers due to the large density of states of the dimer fragment intermolecular vibrational modes, and therefore we compared the observed distributions to predictions of the statistical PST, as well as to QCT calculations. In the PST calculations D_0 was the only parameter used in the fit, and we selected a value that best fit both the shapes of the distributions and their cutoff values. The E_t distributions calculated by PST have no unique structural features. They were converted to speed distributions and compared with the experimental results in Figure 10.

A best fit D_0 and uncertainty were obtained for each image, and we arrive at a final value of D_0 = 2650 ± 150 cm^{-1}, which is in good agreement with the calculated value of 2726 ± 30 cm^{-1} [99]. By comparing this value with that of twice the D_0 value of the water dimer, i.e. ~1105 × 2 cm^{-1}, we estimate that the cooperative (non-additive) interaction contributes 450–500 cm^{-1}. We can now compare this value with the *ab initio* calculations of D_0 for breaking all three hydrogen bonds of $(H_2O)_3$, which is 3855 ± 20 cm^{-1}. This value is 1129 cm^{-1} higher than the calculated value for breaking two H-bonds; a difference that is similar to the value of breaking a single hydrogen bond of $(H_2O)_2$. We conclude, therefore, that the cooperative effect is revealed by observing the $(H_2O)_3 \rightarrow H_2O + (H_2O)_2$ dissociation channel, which breaks the cyclic structure.

We have confirmed the statistical nature of the observed distributions by comparing them to QCT calculations. The translational energy distributions were calculated by QCT using several established methods to account for the ZPE constraint in the fragments. Figure 11a shows a comparison between the measured c. m. E_t distribution obtained in VMI by detecting H_2O fragments in $J''_{KaKc} = 3_{2,1}$ level and the distributions obtained by QCT calculations where the H_2O fragments are in J'' = 2–4. These rotational levels have maximum population, and thus a fairly large number of trajectories are associated with them. The agreement between theory and experiment is encouraging. The QCT calculation also agrees well with PST predictions (Figure 11b).

The PST and QCT distributions for the other degrees of freedom also agree fairly well, confirming the statistical nature of the energy distributions. The more statistical outcome is easily rationalized by the large vibrational density of states in the $(H_2O)_2$ fragment. The harmonic intermolecular vibrational energies of the dimer range from 90 to ~600 cm^{-1}, with 4 of the 6 intermolecular modes being below 300 cm^{-1}. The density of vibrational states can reach >8/cm^{-1} for $(H_2O)_2$ fragments with low rotational and translational energies. In future experiments, it will be interesting to examine and compare the energy distributions of the $(H_2O)_3 \rightarrow 3H_2O$ dissociation channel as well.

The QCT calculations show, as expected, much internal isomerization of the trimer prior to dissociation. The ring opens early on in the trajectory, indicating the breaking of one H-bond. It then reforms and breaks and reforms and breaks (often with different H-bonds breaking) until finally the second H-bond breaks and fragmentation is seen. This evolution is similar to what was inferred

from spectroscopic studies of trimers of HF, DF and HCl [100–102]. In these studies it was concluded that the first step in the dissociation is opening of the ring, followed by further intramolecular vibrational redistribution and finally elimination of a monomer fragment. The timescales, however, differ from case to case.

Finally, to obtain an estimate of the average QCT lifetime of dissociation to dimer + monomer, the distribution of lifetimes for nearly 20 000 trajectories (with no constraints) that dissociated was determined. About 84% of the trajectories that dissociated did so within 10.5 ps. The fairly long lifetimes allow ample time for intramolecular vibrational energy redistribution among close lying rovibrational levels, and complex vibrational motions are indeed observed in the trajectories.

4. Dimers of H_2O with HCl and NH_3

4.1. HCl–H_2O dimer: nonstatistical rotational distributions

The HCl–H_2O dimer is a prototype of H-bonded mixed clusters with an acid. The mechanism of HCl solvation in water is of fundamental importance in physical chemistry, because of the efficient dissociative ionization of HCl [103–116]. HCl interactions with small ice particles are relevant to the chemistry of the upper atmosphere, as is its inelastic scattering from and adsorption onto thin films of water and other solvents [117]. It is thus no wonder that much theoretical and experimental effort has been devoted to understanding the interactions of HCl in diverse environments. However, many questions remain open regarding the dissociation, ionization and energy transfer pathways involving HCl and water.

The HCl–H_2O minimum energy structure has a nearly-linear hydrogen bond (<OHCl $\approx 178^\circ$), with the HCl acting as donor to the oxygen of water [113,118–120]. Despite the ongoing interest in the dimer, there has been no experimental determination of the strength of its hydrogen bond. There exist, however, a number of *abinitio* calculations of D_0. A fairly recent calculation at the CCSD/aug-cc-pVDZ+ level of theory/basis set, for example, gave $D_0 = 1189\ cm^{-1}$[103]. Other calculated values ranged between 1100 and 1570 cm^{-1}[112,115].

We first completed the 'easy' experiment: we excited the intramolecular HCl fundamental vibration at 2723 cm^{-1} and obtained the REMPI spectrum of HCl fragments. We then recorded images of several HCl(J) states to determine D_0. By fitting the broad but distinct structures in multiple images and their energy cutoffs we determined $D_0 = 1334 \pm 10\ cm^{-1}$. This value can now serve as a benchmark for high level calculations. In fact, Mancini and Bowman just reported a new *ab initio* PES and performed Diffusion Monte Carlo calculations to obtain $D_0 = 1348 \pm 3\ cm^{-1}$[121], in good agreement with the experimental results.

We proceeded to detect H_2O directly by 2 + 1 REMPI, as described in Section 2. From each image we extracted the c.m. velocity (speed) distribution, which showed several well-resolved structures assigned unambiguously to specific rotational levels of the HCl cofragment (See Figure 4) We could fit the structures and the cutoffs in the velocity distribution with the same D_0 value obtained by monitoring HCl, thereby validating the water detection scheme.

The available energy was sufficient to excite only rotational levels of the fragments, and we carried out comparisons of the pair-correlated energy distributions with PST. The rotational state distributions of both the water and HCl cofragments were broad, encompassing all allowed levels, but they deviated significantly from the predictions of PST, with overpopulation in high rotational levels (see Figure 12). This has turned out to be a general trend and is in agreement with the Ewing model. The available energy is distributed more evenly among the water cofragment rotational levels than in HCl apparently because there are >50 J''_{KaKc} levels of water, many of which are closely spaced, whereas a maximum of only 12 HCl rotational levels are energetically allowed. The closer spacing of energy levels of H_2O facilitates energy transfer in the exit channel, which leads to spreading the rotational energy more evenly.

4.2. NH_3–H_2O dimer: fragment vibrational state specificity

We have described above the vibrational state specificity in the VP of the water dimer, in which bending excitation in one fragment was the preferred channel. An even clearer example of vibrational state specificity is provided by the NH_3–H_2O dimer and other dimers of ammonia with polyatomic molecules. In the VP of these dimers, a larger number of vibrational levels can be populated, and in this section we briefly discuss the observed vibrational state specificity.

Ammonia is of fundamental interest as a Lewis base, a solvent, and a constituent in solar icy bodies [122]. Mixtures of ammonia and water are important as components of the surfaces of Neptune and Uranus [51], in atmospheric chemistry [123], and in astrochemistry in gas eruptions in icy bodies detected by the Gemini telescope and the Cassini mission [124–128]. Aggregates of water and ammonia are more stable than the corresponding homo-clusters and this is important in mixed ammonia–water ices [45–48,128]. NH_3–H_2O has been the subject of numerous theoretical studies [45–48], but very little was known experimentally about the dimer and its VP dynamics. It has a typical, near-linear, H-bond with the water moiety being the donor.

Upon excitation of NH_3–H_2O in the H-bonded OH stretch (3485 cm^{-1}) [55], a small fraction of NH_3 fragments are generated in the ground state, but mostly they are excited with one or two quanta in the ν_2 bending (umbrella) mode. The rotational energy in each vibrational level is approximated between 250–350 cm^{-1}, with high rotational levels over- populated. The pair correlated E_t distributions determined from images of selected $NH_3(\upsilon_2 = 1, 2,$

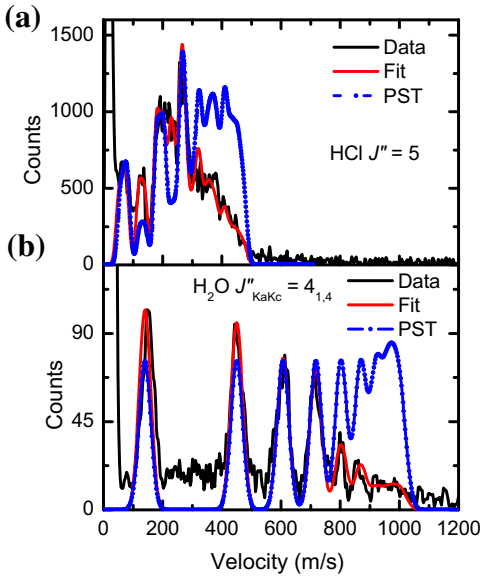

Figure 12. Velocity distributions (black curves) from reconstructed images obtained by monitoring: (a) HCl and (b) H_2O fragments from VP of HCl–H_2O. The red curves correspond to best fits to the data and the blue curves depict statistical distributions obtained by PST. For the fitting, the intensities of the individual gaussians were first generated using an exponential smooth function, and then the gaussian heights were adjusted individually to achieve best fits. The PST calculations, which were done using the same D_0, clearly show that the experimental velocity distributions are non-statistical.

J,K) levels are well simulated with water fragement (J, K_a, K_c) levels whose populations increase for channels with low E_t. From fitting about 20 images of $NH_3(v_2 = 1, 2, J, K)$ fragments, $D_0 = 1538 \pm 10\ cm^{-1}$ was determined [55].

Although the rotational energy distributions show the same propensity for excess population in high rotational levels as do the other dimers discussed above, the vibrational distributions show a yet unexplained state specificity. For example, the asymmetric bend, $\nu_4 \sim 1400\ cm^{-1}$, is not populated, even though there is sufficient energy for its generation (see Figure 13) and this pathway would minimize E_t release.

For NH_3 fragments generated in the ground vibrational state, Ewing rules would favor formation of water co-fragments with one quantum in the bending mode ($\sim$1600 cm^{-1}), which would leave $E_t < 300\ cm^{-1}$ (Figure 13). Nevertheless, as the E_t distribution in Figure 14 shows, most if not all water products are formed in the ground vibrational state, accompanied by E_t release of up to $\sim$1900 cm^{-1}. This is quite surprising because the ammonia fragment $v_2 = 2^+$ level, which has a similar energy, is populated. Although it is possible to speculate on the reasons for this vibrational state specificity, no theoretical model is yet available.

It is instructive to compare the fragment vibrational distributions to those obtained in other ammonia containing dimers that were studied in detail, i.e. $(NH_3)_2$ and NH_3–C_2H_2 [53 129]. Each dimer exhibits vibrational state specificity, but each one has a different vibrational distribution. In the ammonia-acetylene dimer, acetylene acts as the Lewis acid whose hydrogen is weakly bonded to the nitrogen of ammonia ($D_0 = 900 \pm 10\ cm^{-1}$) [53]. Following asym-CH stretch excitation at 3213.6 cm^{-1}, the predominant dissociation channel has NH_3 with one quantum in the umbrella mode v_2, with bending levels (v_4 and/or v_5) of C_2H_2 always excited as well to minimize E_t release. The predominant predissociation channel is $NH_3(1v_2) + C_2H_2(2v_4$ or $1v_4 + 1v_5)$, though a minor channel, $NH_3(2v_2) + C_2H_2(1v_4)$, is also observed. No NH_3 fragment in the ground vibrational state has been identified. Other combinations of fragment states that give rise to low E_t release are not populated, most notably the acetylene C≡C stretch and the ammonia asymmetric bend. It is interesting to note that all the observed channels involve energy transfer across the H-bond. In all cases, rotational excitation in NH_3 fragments is modest, and translational energy release is minimized.

In a recent study, using the same experimental approach, Case et al. determined D_0 and dissociation pathways for the ammonia dimer [129]. This dimer is much more weakly bound than NH_3–H_2O ($D_0 = 660 \pm 20\ cm^{-1}$) and is very floppy, but the same propensity of populating the umbrella mode is exhibited, with population up to the highest allowed bending (umbrella) state,

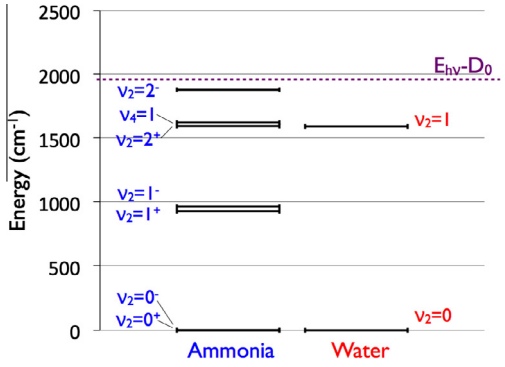

Figure 13. Accessible vibrational levels in the monomer fragments following vibrational predissociation of the NH_3–H_2O dimer via excitation of the H-bonded OH stretch. [Adapted with permission from Ref. [55] (Copyright 2009 American Chemical Society)].

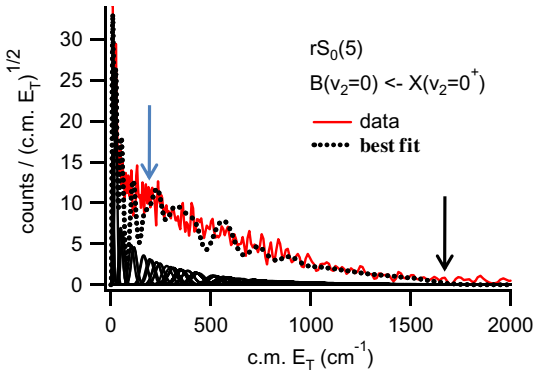

Figure 14. Translational energy distribution (red) obtained by monitoring NH_3 fragment [$v_2 = 0^+$, $^{\Delta K}\Delta J_K(J) = {}^rS_0(5)$] via the $\tilde{B} \leftarrow \tilde{X}$ transition in the VP of NH_3–H_2O. The dotted black line corresponds to the best fit to the data. The maximum available translational energy with and without one quantum of bending excitation in the water cofragment are indicated by blue and black arrows, respectively. [Adapted with permission from Ref. [55] (Copyright 2009 American Chemical Society)].

$v_2 = 3$. However, in all cases there are at least 2 quanta of bending excitation in the fragments, in accordance with the momentum gap law. As in the other cases, the asymmetric bend ν_4 is not populated, and the rotational excitations are nonstatistical.

5. Conclusions and perspective

We have described above new studies of H-bond breaking in small clusters that include water. In addition to measuring bond dissociation energies with spectroscopic accuracy, we were intrigued by the state specificity exhibited in the predissociation dynamics and the intramolecular vibrational redistribution in the fragments. Although dynamical calculations are difficult (for the reasons stated above), the synergy between experiment and theory can lead to fast progress by testing approximations and enabling extensions to larger systems. The pioneering quasi-classical trajectory calculations of Czakó, Wang, and Bowman have described aspects of VP that are complementary to the experiments, and thus provided a more complete picture of the mechanisms. These studies can be extended to other small mixed dimers for which accurate PESs exist.

Several common motifs are apparent in the VP of dimers, some of which recognized in the past. The inefficiency of energy transfer from high-frequency intramolecular stretch vibrations to intermolecular modes is well understood in terms of the momentum gap law, as is the propensity to minimize translational energy release.

The floppiness of the dissociating dimers is demonstrated by the J, K rotational distributions of the fragments. When we tried to model the pair-correlated velocity distributions with distributions that included constraints on K states (or K_a/K_c states in water), we obtained a much more structured distribution than observed experimentally. Likewise, modeling the REMPI spectra of fragments with distributions that include a preference for $K = 0$ or $K = J$ did not match the experimental measurements. Thus, no specific orientations of the K vectors relative to J of the fragments are favored. This is borne out by trajectory calculations of the VP of the water dimer, which show unrestricted tumbling before dissociation. The calculated vector correlations, however, do show a tendency for J to be perpendicular to the velocity vector v [60], reflecting the planar orientation in the dimer at long inter-monomer separations, as expected for electrostatic attraction. Note that the classical trajectories do not include K.

What is not explained yet is the state specificity in vibrational energy flow in dimers, which persists in spite of the slowness of the H-bond breaking. Clearly, only specific pathways lead to dissociation, and those differ from case to case. In some cases this might be rationalized by classical arguments of force and torque combined with the need to form products with vibrational and rotational excitations that minimize translational energy release [57], but evidently this is not the whole story. For example, consider the fragment vibrational distribution in the VP of $(H_2O)_2$ and NH_3–H_2O. In both dimers the H-bonded OH-stretch vibration is excited, but in the former the water fragment bend is predominantly excited, whereas in the latter case it is only the umbrella mode of the ammonia fragment that is excited. Fragments in which the water bend is excited are at best a minor channel, even though this is the channel for which the Ewing propensity rules are satisfied the best. It appears that the coupling strengths with the intermolecular bonds play an important role in determining the fragment vibrational distributions.

From an experimental perspective, the studies described here are challenging because of the need to excite selectively a specific cluster and have an efficient REMPI detection system for the products. HCl and NH_3 can be detected straightforwardly (though their excited states are predissociative), but the detection of water must be improved if this method is to be extended to higher clusters of water. Also, while it is fairly easy to find experimental conditions that optimize formation of dimers in the expansion, extensions to trimers and other clusters are more challenging. We believe, however, that it is feasible to detect higher clusters of water and also trimers that include ammonia and HCl. Such experiments would enable us to interrogate H-bond networks that have bent or distorted H-bonds, situations similar to those that exist in liquid water, as well as assess the contributions of cooperative interactions. We hope that these studies will inspire further theoretical efforts as well, as demonstrated by the recent success of QCT calculations on the VP of the water dimer and trimer.

Acknowledgments

The research described in this Letter was inspired by the pioneering studies of the late Roger Miller on the predissociation dynamics of small clusters. It benefitted greatly from the theoretical work of Bowman and coworkers that served as the motivation to extend our work to the water dimer and trimer. We thank our collaborators and coworkers for their essential contributions and for many enlightening discussions: Anthony McCaffery, Joel Bowman, Jessica Parr, Guosheng Li, Andrew Mollner, Blithe Rocher, Gábor Czakó and Yimin Wang. This research was supported by the US National Science Foundation Grant CHE-0951976.

References

[1] W.M. Latimer, W.H. Rodebush, J. Am. Chem. Soc. 42 (1920) 1419.
[2] J.D. Bernal, R.H. Fowler, J. Chem. Phys. 1 (1933) 515.
[3] J.D. Bernal, Proc. R. Soc. London, A 280 (1964) 299.
[4] L. Pauling, Proc. Natl. Acad. Sci. USA 14 (1928) 359.
[5] L. Pauling, The Nature of the Chemical Bond and the Structure of Molecules and Crystals: An Introduction to Modern Structural Chemistry, Cornell University Press, New York, 1939.
[6] S. Scheiner, New York, Cornell Univ. Press, 1997.
[7] T. Steiner, Angew. Chem. Int. Ed. 41 (2002) 48.
[8] T.S. Zwier, Annu. Rev. Phys. Chem. 47 (1996) 205.
[9] A. Rohrbacher, N. Halberstadt, K.C. Janda, Annu. Rev. Phys. Chem. 51 (2000) 405.
[10] L. Oudejans, R.E. Miller, Annu. Rev. Phys. Chem. 52 (2001) 607.
[11] J.M. Hutson, Annu. Rev. Phys. Chem. 41 (1990) 123.
[12] M.C. Heaven, Annu. Rev. Phys. Chem. 43 (1992) 283.
[13] S. Scheiner, Annu. Rev. Phys. Chem. 45 (1994) 23.
[14] D.J. Nesbitt, Annu. Rev. Phys. Chem. 45 (1994) 367.
[15] D.J. Miller, J.M. Lisy, J. Am. Chem. Soc. 130 (2008) 15381.
[16] D.J. Miller, J.M. Lisy, J. Am. Chem. Soc. 130 (2008) 15393.
[17] A.S. Pine, W.J. Lafferty, J. Chem. Phys. 78 (1983) 2154.
[18] R.E. Miller, Acc. Chem. Res. 23 (1990) 10.
[19] Z.S. Huang, R.E. Miller, J. Chem. Phys. 86 (1987) 6059.
[20] Z.S. Huang, R.E. Miller, J. Chem. Phys. 90 (1989) 1478.
[21] D.T. Moore, L. Oudejans, R.E. Miller, J. Chem. Phys. 110 (1999) 197.
[22] L. Oudejans, D.T. Moore, R.E. Miller, J. Chem. Phys. 110 (1999) 209.
[23] A.S. Pine, W.J. Lafferty, B.J. Howard, J. Chem. Phys. 81 (1984) 2939.
[24] V. Vaida, J. Chem. Phys. 135 (2011) 020901.
[25] Y. Scribano, N. Goldman, R.J. Saykally, C. Leforestier, J. Phys. Chem. A 110 (2006) 5411.
[26] N. Goldman, C. Leforestier, R.J. Saykally, J. Phys. Chem. A 108 (2004) 787.
[27] N. Goldman, R.S. Fellers, C. Leforestier, R.J. Saykally, J. Phys. Chem. A 105 (2001) 515.
[28] C. Leforestier, K. Szalewicz, A. van der Avoird, J. Chem. Phys. 137 (2012) 014305.
[29] H.G. Kjaergaard, A.L. Garden, G.M. Chaban, R.B. Gerber, D.A. Matthews, J.F. Stanton, J. Phys. Chem. A 112 (2008) 4324.
[30] J.R. Lane, V. Vaida, H.G. Kjaergaard, J. Chem. Phys. 128 (2008).
[31] J. Millan, N. Halberstadt, G. van der Sanden, A. van der Avoird, J. Chem. Phys. 114 (2001) 6487.
[32] P. Carcabal, V. Brenner, N. Halberstadt, P. Millie, Chem. Phys. Lett. 336 (2001) 335.
[33] M.W. Aviles, M.L. McCandless, E. Curotto, J. Chem. Phys. 128 (2008) 124517.
[34] Y. Watanabe, S. Maeda, K. Ohno, J. Chem. Phys. 129 (2008) 074315.
[35] R. Hernandez-Lamoneda, V.H.U. Rosas, M.I.B. Uruchurtu, N. Halberstadt, K.C. Janda, J. Phys. Chem. A 112 (2008) 89.
[36] R. Kumar, J.L. Skinner, J. Phys. Chem. B 112 (2008) 8311.
[37] M. Geleijns, N. Halberstadt, J. Millan, P.E.S. Wormer, A. van der Avoird, Faraday Discuss. 118 (2001) 143.
[38] M.E. Dunn, T.M. Evans, K.N. Kirschner, G.C. Shields, J. Phys. Chem. A 110 (2006) 303.
[39] Y. Kim, J. Phys. Chem. A 110 (2006) 600.
[40] P.E.S. Wormer, A. van der Avoird, Chem. Rev. 100 (2000) 4109.
[41] Y. Wang, S. Carter, B.J. Braams, J.M. Bowman, J. Chem. Phys. 128 (2008) 71101.
[42] X. Huang, B.J. Braams, J.M. Bowman, R.E.A. Kelly, J. Tennyson, G.C. Groenenboom, A. van Der Avoird, J. Chem. Phys. 128 (2008) 034312.
[43] X.C. Huang, B.J. Braams, J.M. Bowman, J. Phys. Chem. A 110 (2006) 445.
[44] N. Goldman, C. Leforestier, R.J. Saykally, Philos. Trans. R. Soc. London, A 363 (2005) 493.
[45] J. Sadlej, R. Moszynski, J.C. Dobrowolski, A.P. Mazurek, J. Phys. Chem. A 103 (1999) 8528.
[46] J. Rzepkowska, N. Uras, J. Sadlej, V. Buch, J. Phys. Chem. A 106 (2002) 1790.
[47] A.D. Fortes, J.P. Brodholt, I.G. Wood, L. Vocadlo, H.D.B. Jenkins, J. Chem. Phys. 115 (2001) 7006.
[48] A.D. Fortes, J.P. Brodholt, I.G. Wood, L. Vocadlo, J. Chem. Phys. 118 (2003) 5987.
[49] Y. Bouteiller, J.P. Perchard, Chem. Phys. 305 (2004) 1.
[50] R.S. Smith, N.G. Petrik, G.A. Kimmel, B.D. Kay, Acc. Chem. Res. 45 (2012) 33.
[51] C. Cavazzoni, G.L. Chiarotti, S. Scandolo, E. Tosatti, M. Bernasconi, M. Parrinello, Science 283 (1999) 44.
[52] G.S. Li, J. Parr, I. Fedorov, H. Reisler, Phys. Chem. Chem. Phys. 8 (2006) 2915.
[53] J.A. Parr, G. Li, I. Fedorov, A.J. McCaffery, H. Reisler, J. Phys. Chem. A 111 (2007) 7589.
[54] M. Pritchard, J. Parr, G.S. Li, H. Reisler, A.J. McCaffery, Phys. Chem. Chem. Phys. 9 (2007) 6241.
[55] A.K. Mollner, B.E. Casterline, L.C. Ch'ng, H. Reisler, J. Phys. Chem. A 113 (2009) 10174.
[56] B.E. Casterline, A.K. Mollner, L.C. Ch'ng, H. Reisler, J. Phys. Chem. A 114 (2010) 9774.
[57] A.J. McCaffery, M. Pritchard, H. Reisler, J. Phys. Chem. A 114 (2010) 2983.
[58] B.E. Rocher-Casterline, A.K. Mollner, L.C. Ch'ng, H. Reisler, J. Phys. Chem. A 115 (2011) 6903.
[59] B.E. Rocher-Casterline, L.C. Ch'ng, A.K. Mollner, H. Reisler, J. Chem. Phys. 134 (2011) 211101.
[60] L.C. Ch'ng, A.K. Samanta, J. Am. Chem. Soc. 134 (2012) 15430.
[61] H. Reisler, Annu. Rev. Phys. Chem. 60 (2009) 39.
[62] G.E. Ewing, J. Chem. Phys. 72 (1980) 2096.
[63] G.E. Ewing, J. Phys. Chem. 91 (1987) 4662.
[64] A.J. McCaffery, R.J. Marsh, J. Chem. Phys. 117 (2002) 9275.
[65] A.J. McCaffery, Phys. Chem. Chem. Phys. 6 (2004) 1637.
[66] P. Pechukas, J.C. Light, J. Chem. Phys. 42 (1965) 3281.
[67] P. Pechukas, J.C. Light, C. Rankin, J. Chem. Phys. 44 (1966) 794.
[68] J.C. Light, J. Lin, J. Chem. Phys. 43 (1965) 3209.
[69] V. Dribinski, A. Ossadtchi, V.A. Mandelshtam, H. Reisler, Rev. Sci. Instrum. 73 (2002) 2634.
[70] A. Eppink, D.H. Parker, Rev. Sci. Instrum. 68 (1997) 3477.
[71] V. Dribinski, A.B. Potter, I. Fedorov, H. Reisler, J. Chem. Phys. 121 (2004) 12353.
[72] F.N. Keutsch, R.S. Fellers, M.G. Brown, M.R. Viant, P.B. Petersen, R.J. Saykally, J. Am. Chem. Soc. 123 (2001) 5938.
[73] F.N. Keutsch, L.B. Braly, M.G. Brown, H.A. Harker, P.B. Petersen, C. Leforestier, R.J. Saykally, J. Chem. Phys. 119 (2003) 8927.
[74] F.N. Keutsch, J.D. Cruzan, R.J. Saykally, Chem. Rev. 103 (2003) 2533.
[75] J.B. Paul, R.A. Provencal, C. Chapo, K. Roth, R. Casaes, R.J. Saykally, J. Phys. Chem. A 103 (1999) 2972.

[76] C.H. Yang, G. Sarma, J.J. ter Meulen, D.H. Parker, C.M. Western, Phys. Chem. Chem. Phys. 12 (2010) 13983.
[77] T. Nakayama et al., J. Chem. Phys. 127 (2007) 134302.
[78] C. Leforestier, R. van Harrevelt, A. van der Avoird, J. Phys. Chem. A 113 (2009) 12285.
[79] J.K. Gregory, D.C. Clary, J. Phys. Chem. 100 (1996) 18014.
[80] W. Klopper, J. van Duijneveldt-van de Rijdt, F.B. van Duijneveldt,, Phys. Chem. Chem. Phys. 2 (2000) 2227.
[81] A. Shank, Y.M. Wang, A. Kaledin, B.J. Braams, J.M. Bowman, J. Chem. Phys. 130 (2009) 144314.
[82] G.S. Tschumper, M.L. Leininger, B.C. Hoffman, E.F. Valeev, H.F. Schaefer, M. Quack, J. Chem. Phys. 116 (2002) 690.
[83] G. Czakó, Y. Wang, J.M. Bowman, J. Chem. Phys. 135 (2011) 151102.
[84] C. Leforestier, Philos. Trans. R. Soc. London, A 370 (2012) 2675.
[85] L.C. Ch'ng, A.K. Samanta, Y. Wang, J.M. Bowman, H. Reisler, J. Phys. Chem. A, http://dx.doi.org/10.1021/jp401155v.
[86] J.A. Anderson, K. Crager, L. Fedoroff, G.S. Tschumper, J. Chem. Phys. 121 (2004) 11023.
[87] B. Santra, A. Michaelides, M. Scheffler, J. Chem. Phys. 127 (2007) 184104.
[88] A. van der Avoird, K. Szalewicz, J. Chem. Phys. 128 (2008) 014302.
[89] P.T. Kiss, A. Baranyai, J. Chem. Phys. 131 (2009) 204310.
[90] T. Salmi, H.G. Kjaergaard, L. Halonen, J. Phys. Chem. A 113 (2009) 9124.
[91] G. Czakó, A.L. Kaledin, J.M. Bowman, Chem. Phys. Lett. 500 (2010) 217.
[92] T. Salmi, E. Sälli, L. Halonen, J. Phys. Chem. A 116 (2012) 5368.
[93] F. Huisken, M. Kaloudis, A. Kulcke, J. Chem. Phys. 104 (1996) 17.
[94] J.B. Paul, C.P. Collier, R.J. Saykally, J.J. Scherer, A. Okeefe, J. Phys. Chem. A 101 (1997) 5211.
[95] L.B. Braly, K. Liu, M.G. Brown, F.N. Keutsch, R.S. Fellers, R.J. Saykally, J. Chem. Phys. 112 (2000) 10314.
[96] M.N. Slipchenko, K.E. Kuyanov, B.G. Sartakov, A.F. Vilesov, J. Chem. Phys. 124 (2006) 241101.
[97] C.J. Burnham, S.S. Xantheas, M.A. Miller, B.E. Applegate, R.E. Miller, J. Chem. Phys. 117 (2002) 1109.
[98] A. Moudens, R. Georges, M. Goubet, J. Makarewicz, S.E. Lokshtanov, A.A. Vigasin, J. Chem. Phys. 131 (2009) 204312.
[99] Y. Wang, J.M. Bowman, J. Chem. Phys. 135 (2011) 131101.
[100] D.W. Michael, J.M. Lisy, J. Chem. Phys. 85 (1986) 2528.
[101] M.A. Suhm, J.T. Farrell, S.H. Ashworth, D.J. Nesbitt, J. Chem. Phys. 98 (1993) 5985.
[102] M. Farnik, D.J. Nesbitt, J. Chem. Phys. 121 (2004) 12386.
[103] S. Odde, B.J. Mhin, S. Lee, H.M. Lee, K.S. Kim, J. Chem. Phys. 120 (2004) 9524.
[104] D. Skvortsov, S.J. Lee, M.Y. Choi, A.F. Vilesov, J. Phys. Chem. A 113 (2009) 7360.
[105] S.D. Flynn, D. Skvortsov, A.M. Morrison, T. Liang, M.Y. Choi, G.E. Douberly, A.F. Vilesov, J. Phys. Chem. Lett. 1 (2010) 2233.
[106] A.M. Morrison, S.D. Flynn, T. Liang, G.E. Douberly, J. Phys. Chem. A 114 (2010) 8090.
[107] A. Gutberlet et al., Science 324 (2009) 1545.
[108] W.H. Robertson, M.A. Johnson, Science 298 (2002) 69.
[109] H. Forbert, M. Masia, A. Kaczmarek-Kedziera, N.N. Nair, D. Marx, J. Am. Chem. Soc. 133 (2011) 4062.
[110] M. Masia, H. Forbert, D. Marx, J. Phys. Chem. A 111 (2007) 12181.
[111] L. Walewski, H. Forbert, D. Marx, J. Phys. Chem. Lett. 2 (2011) 3069.
[112] M.J. Packer, D.C. Clary, J. Phys. Chem. 99 (1995) 14323.
[113] M.E. Alikhani, B. Silvi, Phys. Chem. Chem. Phys. 5 (2003) 2494.
[114] G.M. Chaban, R.B. Gerber, K.C. Janda, J. Phys. Chem. A 105 (2001) 8323.
[115] S. Re, Y. Osamura, Y. Suzuki, H.F. Schaefer, J. Chem. Phys. 109 (1998) 973.
[116] A. Milet, C. Struniewicz, R. Moszynski, P.E.S. Wormer, J. Chem. Phys. 115 (2001) 349.
[117] S.M. Brastad, G.M. Nathanson, Phys. Chem. Chem. Phys. 13 (2011) 8284.
[118] A.J. Huneycutt, R.J. Stickland, F. Hellberg, R.J. Saykally, J. Chem. Phys. 118 (2003) 1221.
[119] Z. Kisiel, B.A. Pietrewicz, P.W. Fowler, A.C. Legon, E. Steiner, J. Phys. Chem. A 104 (2000) 6970.
[120] A.C. Legon, L.C. Willoughby, Chem. Phys. Lett. 95 (1983) 449.
[121] J.S. Mancini, J.M. Bowman, Chem. Phys 138 (2013) 121102.
[122] M.L. Clapp, R.E. Miller, Icarus 105 (1993) 529.
[123] D.J. Donaldson, J. Phys. Chem. A 103 (1999) 62.
[124] M.E. Brown, W.M. Calvin, Science 287 (2000) 107.
[125] J.C. Cook, S.J. Desch, T.L. Roush, C.A. Trujillo, T.R. Geballe, Astrophys. J. 663 (2007) 1406.
[126] M.H. Moore, R.F. Ferrante, R.L. Hudson, J.N. Stone, Icarus 190 (2007) 260.
[127] A.J. Verbiscer et al., Icarus 182 (2006) 211.
[128] W. Zheng, D. Jewitt, R.I. Kaiser, Astrophys. J. 181 (2009) 53.
[129] A.S. Case, C.G. Heid, S.H. Kable, F.F. Crim, J. Chem. Phys. 135 (2011) 084312.

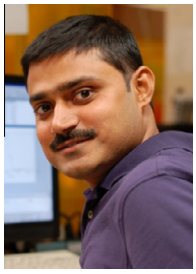

Amit K. Samanta obtained his B.Sc. and M.Sc. degrees in Chemistry from the University of Calcutta, India. In 2010, he received his Ph.D. from the Indian Association for the Cultivation of Science (IACS), India, working under the supervision of Prof. Tapas Chakraborty. His doctoral work involved studies of cooperative and anti-cooperative effects in interconnected hydrogen bonded networks using matrix isolation infrared spectroscopy. In 2011, he joined the Reisler group as a postdoctoral researcher and is currently working on the predissociation dynamics of hydrogen bonded clusters using velocity map imaging.

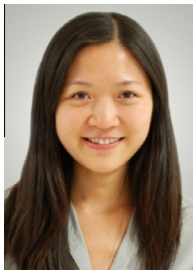

Lee Chiat Ch'ng received her B.S. in Chemistry at Linfield College in 2007. She then joined the Department of Chemistry at the University of Southern California. Her graduate research is conducted under the direction of Professor Hanna Reisler and focuses on imaging hydrogen bond breaking in small water clusters. She is the recipient of the Skinner Prize for her poster presentation at the Faraday Discussion No. 157 and a poster award at the International Chemistry Congress of the Pacific Basin Societies.

Hanna Reisler received her Ph.D. in Physical Chemistry from the Weizmann Institute of Science in Israel in 1972. After postdoctoral training at the Johns Hopkins University (1972-1974) she held several research positions before joining the Department of Chemistry at USC in 1987, where she is now the holder of the Lloyd Armstrong Jr. Chair in Science and Engineering. Her research interests are in the areas of chemical reaction dynamics and photochemistry. She is a Fellow of the American Physical Society and the American Association for the Advancement of Science. She received a Max Planck Research Award in 1994 and the Broida Prize of the American Physical Society in 2005.